2002-10-01

Compact focusing von Hamos spectrometer for quantitative x-ray spectroscopy

Larry V. Knight
larry_knight@byu.edu

A. P. Shevelko

Yu S. Kasyanov

O. F. Yakushev

Original Publication Citation

Shevelko, A. P., Yu, O. F. Yakushev, and L. V. Knight."Compact focusing von Hamos spectrometer for quantitative x-ray spectroscopy." Review of Scientific Instruments 73 (22): 3458-3463.

Compact focusing von Hamos spectrometer for quantitative x-ray spectroscopy

A. P. Shevelko, Yu. S. Kasyanov, and O. F. Yakushev
Optical Division, P. N. Lebedev Physical Institute of the Russian Academy of Sciences, Moscow 117924, Russia

L. V. Knight[a)]
Department of Physics and Astronomy, Brigham Young University, Provo, Utah 84602

(Received 25 September 2001; accepted for publication 2 June 2002)

A compact focusing crystal spectrometer based on the von Hamos scheme is described. Cylindrically curved mica and graphite crystals with a radius of curvature of $R=20$ mm are used in the spectrometer. A front illuminated charge-coupled device (CCD) linear array detector makes this spectrometer useful for real-time spectroscopy of laser-produced plasma x-ray sources within the wavelength range of $\lambda=1.8-10$ Å. Calibration of crystals and the CCD linear array makes it possible to measure absolute photon fluxes. X-ray spectra in an absolute intensity scale were obtained from Mg, Ti, and Fe laser-produced plasmas, with a spectral resolution $\lambda/\delta\lambda=800-2000$ for the mica and $\lambda/\delta\lambda=200-300$ for graphite crystal spectrometers. The spectrometer has high efficiency in a wide spectral range, it is compact (40 mm diam, 150 mm length), easy to align, and flexible. The spectrometer is promising for absolute spectral measurements of x-ray radiation of low-intensity sources (femtosecond laser-produced plasmas, micropinches, electron-beam–ion-trap sources, etc.). © *2002 American Institute of Physics.*
[DOI: 10.1063/1.1502013]

I. INTRODUCTION

The x-ray crystal spectrometer is an important diagnostic tool in x-ray spectroscopy. A good x-ray spectrometer must perform two functions:

- Estimate photon flux from x-ray sources—this requires the absolute calibration of the spectrometer sensitivity.
- The measurement of low-intensity x-ray lines—this can be achieved by using focusing crystal x-ray spectrometers and by using x-ray detectors with high quantum efficiency.

Charge-coupled devices (CCDs) are often used as detectors in soft x-ray imaging systems.[1,2] CCD x-ray detectors have the advantages of high sensitivity, good signal-to-noise ratio, wide dynamic range, and good spatial resolution. In the form of a two-dimensional array detector, CCDs are a suitable replacement for photographic film in spectroscopic instruments. An x-ray sensitive CCD is a good real-time detector with known quantum efficiency and linear response. Examples can be found in Refs. 3–5, where CCDs were used in flat and spherical crystal spectrometers for x-ray spectroscopy of laser-produced plasmas.

The maximum efficiency of x-ray spectroscopic devices for polychromatic radiation can be achieved when a CCD is used in the focusing scheme of crystal x-ray spectrometers. One of these is the von Hamos scheme.[6] This scheme has several advantages—the most important being high efficiency in a wide spectral range. For this reason the von Hamos spectrometer is widely used in studies of various x-ray sources (see the review in Ref. 7). Some examples of these applications are laser-produced plasmas,[7–11] beam–target experiments,[12,13] Tokamak plasmas,[14] electron-beam–ion-trap (EBIT) sources,[15] fluorescence, and scattering experiments.[16] In the von Hamos geometry x-ray spectra are formed on the spectrometer axis. Thus, it is possible to use a simple, low-cost CCD linear array as a detector. In addition, the detector covers a wide spectral range because of the length of the CCD linear array along the dispersion direction.

In this article, we describe a compact crystal spectrometer based on a focusing von Hamos scheme with a CCD linear array as detector. The spectrometer was calibrated absolutely and was used for absolute spectral measurements of laser-produced plasma x-ray sources.

II. VON HAMOS GEOMETRY

In the von Hamos scheme,[6] a crystal is bent into a cylindrical surface. The x-ray source and the detector plane lie on the cylinder axis (Fig. 1). The von Hamos geometry and characteristics are described in detail in Ref. 7. The crystal diffracts x rays with different wavelengths according to Bragg's law. In the von Hamos geometry it is possible to separate two planes: a plane containing a spectrometer axis (the dispersion plane) and a plane perpendicular to the axis. In the dispersion plane, a curved crystal in the von Hamos geometry works like a flat crystal. Different wavelengths are diffracted at different points along the crystal surface and detected at different points along the spectrometer axis. The spectral range $\Delta\lambda/\lambda=\Delta\theta\cot\theta$ depends on the Bragg angle θ and the accepted divergence $\Delta\theta$, which is proportional to

a)Electronic mail: larry_knight@byu.edu

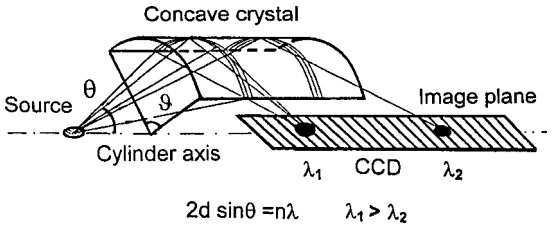

FIG. 1. Schematic diagram of the von Hamos spectrometer: the x-ray source and the detector plane lie on the axis of the cylindrical crystal. Each wavelength, after reflection from the crystal arc, is focused to a point lying on the spectrometer axis.

the crystal length and to the detector length. For the long crystal and large detector length, the wavelength bandwidth $\Delta\lambda$ could be rather wide.

In the plane perpendicular to the spectrometer axis, the von Hamos scheme has a large collection solid angle and focuses the collected radiation. Each wavelength is focused to a unique point on the spectrometer axis (Fig. 1). The relation between exposure I (photons/μm^2) on the image plane in the von Hamos spectrometer and the time-integrated brightness of the monochromatic source L (photons/μm^2 sr) is equal to[7]

$$I = BL\,. \tag{1}$$

The parameter B(sr) is given by

$$B = T\rho\vartheta\sin^2\theta, \tag{2}$$

which defines the spectrometer efficiency [T is the filter transmission, ρ (rad) is the integrated reflectivity, ϑ (rad) is the angular aperture of the spectrometer, and θ is the Bragg angle; see Fig. 1]. The higher B the higher intensity I in the detection plane. The von Hamos focusing geometry gives high spectrometer collection efficiency. For example, the ratio of efficiencies of the von Hamos spectrometer and a flat crystal spectrometer working at the same geometry is equal to[7]

$$R\vartheta/a, \tag{3}$$

where R is the radius of curvature of the crystal, ϑ is the angular aperture of the crystal, and a is a source size. For a small source size this ratio may be as large as 10^2-10^3. This enhanced collection efficiency of a von Hamos spectrometer is attractive for the study of low-intensity, small-size x-ray sources. Note that the von Hamos geometry has focusing properties and, hence, high collection efficiency in a full spectral bandwidth $\Delta\lambda$. In other focusing schemes the wavelength band and efficiency are mutually exclusive.[7] In Johann or Johansson crystal schemes, the realization of maximum efficiency leads to a severe restriction of the recording wavelength bandwidth. For this reason the von Hamos spectrometer is a "polychromator," whereas the others are "monochromators."

The spectra obtained with a von Hamos spectrometer form a two-dimensional image of the source for each wavelength.[6,7] If a CCD linear array is used as an x-ray detector, each CCD pixel integrates the radiation over the pixel height in the direction perpendicular to the dispersion (Fig. 1). Thus, only a one-dimensional image is observed.

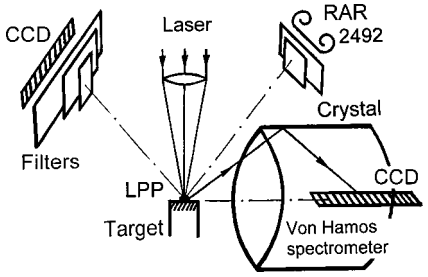

FIG. 2. Diagram of the experiments in which a laser-produced plasma (LPP) is used as the x-ray source. The signal of the CCD linear array is compared with the exposure of absolutely calibrated x-ray photographic film Kodak RAR 2492. The absolutely calibrated CCD is used in the von Hamos spectrometer to record x-ray spectra of laser-produced plasmas.

The width of each spectral line corresponds to the source size. But, at the same time, the integration over the pixel height leads to enhanced spectrometer efficiency.

Another distinctive feature of the von Hamos geometry is that it allows the use of mosaic crystals with highly integrated reflectivity. This further increases spectrometer efficiency. In this case, mosaic parafocusing in the direction of dispersion takes place.[9,16] This results in high sensitivity without sacrificing spectral resolution.[9,10]

III. EXPERIMENTS

The CCD linear arrays was absolutely calibrated: sensitivity, spectral response, and quantum efficiency measurements were made using laser-produced plasmas. Then, absolute x-ray spectral measurements of laser-produced plasmas were performed using the focusing crystal von Hamos spectrometer with a CCD linear array as a detector.

Laser-produced plasmas were created using the "Phoenix" Nd glass laser (the Lebedev Physical Institute) operated at a wavelength of 0.53 μm with pulse energy up to 10 J and 2 ns pulse duration. The laser beam was focused onto massive Mg, Al, Ti, or Fe targets (see Fig. 2). The focal spot diameter was about $\sim$15 μm.

A. CCD

The commercial CCD used for x-ray detection is the Toshiba model TCD 1304AP. It is a linear array with 3724 pixels. Each pixel is 8 μm wide (6 μm active) and 200 μm high. The total detection area is 200 μm by 29.8 mm (8 μm$\times$3724 elements). The front cover glass is removed for x-ray detection. The integration time in the CCD driver program can be varied from 7.6 ms to several hours. We usually used an integration time of 100 ms. At a temperature of 20 °C with an integrating time of 100 ms, the dark current noise, 3σ, is 0.5% of the saturation value.

To prevent visible light illumination, a double Al-coated mylar filter (4.4 μm of mylar, 0.2 μm of Al) was used.

B. CCD calibration

The detector is calibrated by exposing it to monochromatic radiation of known intensity. The comparison of the CCD signal (counts/pixel) with incidence photon flux

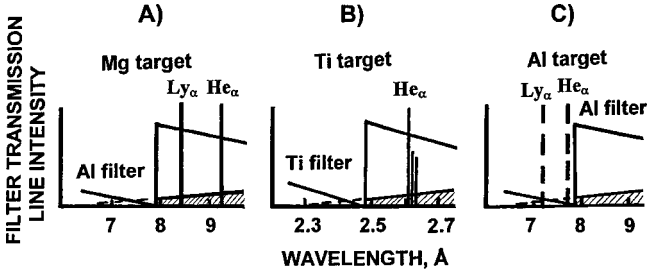

FIG. 3. Principle of wavelength selection in absolute calibration experiments. The positions of resonance lines (Ly_α, He_α) and *K* edges of the x-ray filters are indicated. When the combination of Mg target–Al filters and Ti target–Ti filters are used, filters transmit only resonance lines and continuum radiation (marked as a shaded pedestal) (A) and (B). The contribution of continuum radiation is evaluated using an Al target and Al filters: filters block all line radiation (C).

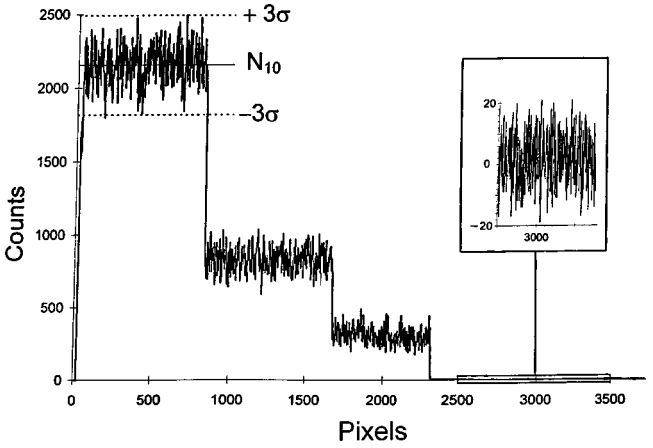

FIG. 4. Example of the CCD x-ray signal (Mg laser-produced plasma, CCD filters: 6.25, 12.5, and 25 μm of Al). In the rectangular frame dark current distribution (noise) is presented (exposure time of 100 ms, CCD temperature of 20 °C).

(photons/pixel) gives the absolute CCD sensitivity, N_0 (photons/count), in each pixel at a given photon energy (wavelength).

Quasimonochromatic radiation from laser-produced plasmas was formed using a combination of target materials and x-ray filters. The method was described earlier for calibration of the von Hamos spectrometer[7,10,11] and is illustrated in Fig. 3. Targets with midrange atomic numbers $Z_a = 12$, 13, and 22 were chosen, so hydrogen- and helium-like ions (H- and He-like ions) were excited in the laser-produced plasmas. The x-ray line radiation of the ions lies in the spectral range of interest (see Table I). X-ray *K*-absorption filters isolated a narrow spectral band with only a few lines. Thus, only the radiation of resonance lines and corresponding satellites of H- and He-like ions were selected by the filters. Systematic error was caused mainly by the contribution of continuum spectra out of the separated spectral band. The x-ray filter also transmitted continuum radiation from the long-wavelength side of the *K* edge (see Fig. 3: a combination of Mg target and Al filter). This contribution was estimated using a combination of an Al target and an Al filter (see Fig. 3). In this case the filter transmitted only continuum radiation from the long-wavelength side of the *K* edge and no line radiation. The measurements showed that the contribution of the continuum radiation did not exceed 20% of the line radiation intensity.

The scheme for the calibration experiments is shown in Fig. 2. The CCD array and a photographic film camera were installed in a vacuum chamber symmetrically with respect to the x-ray source. The same x-ray filters were used in both channels. Filters with the desired spectral band were chosen (see Table I). Kodak RAR 2492 x-ray photographic film measured the absolute x-ray intensity using the absolute calibration data.[17] These data were compared with the CCD signal (see Fig. 4), and the absolute CCD sensitivity, N_0 (photons/count), was determined (see Table I).

The noise performance of a CCD is one of the most important factors because it defines the CCD's detection limit.[2] There are two major noise sources: dark current noise and photon shot noise. The CCD driver program subtracts the dark current background. Figure 4 shows the dark current noise after the background subtraction. 3σ of the noise corresponds to ~20 counts for an exposure time of 100 ms. This value defines the CCD's detection limit, i.e., a minimum exposure $n_{\min}$ (photons/pixel) or $n_{\min}$ (photons/μm^2), which can be detected at this dark current noise level. According to Table I, $3\sigma = 20$ counts correspond to $n_{\min} = 3.6$ photons/pixel for $\lambda = 8.4$–9.2 Å, and $n_{\min} = 1.2$ photons/pixel for $\lambda = 2.6$ Å. These values correspond to exposures $n_{\min} = 3 \times 10^{-3}$ photons/μm^2 and $n_{\min} = 1 \times 10^{-3}$ photons/μm^2 (the pixel area is 6×200 μm^2). These exposures could be compared with the detection limit for the x-ray Kodak RAR 2492 photographic film. The film exposures for optical density $D = 0.1$ are equal to 0.43 and 0.84 photons/μm^2 for the same wavelengths.[17] These estimates show that the CCD is 140–840 times more sensitive than the photographic film.

The other important source of noise is photon shot noise. This noise grows as the incoming photon flux increases. The uncertainty follows a Poisson distribution and its value is proportional to the square root of the number of photons, N_1, depleted in the silicon.[1] The photon shot noise can be used to estimate the quantum efficiency (QE) of the CCD. In Fig. 4, the noise envelope corresponds to $\pm 3\sigma$ of the measurement,

TABLE I. Measured absolute values for CCD sensitivity and CCD quantum efficiency (laser-produced plasma source).

Target	Ions	Filters	Photon energy *E*	N_0, photon/count	N_1 photon/count	QE
Mg	H He	6.25, 12.5, and 25.0 μm Al	1.35–1.5 keV	0.186 ± 0.02	0.15 ± 0.015	0.8
Ti	He	15.9, 31.8, and 47.7 μm Ti	4.8 keV	0.065 ± 0.007	0.056 ± 0.006	0.9

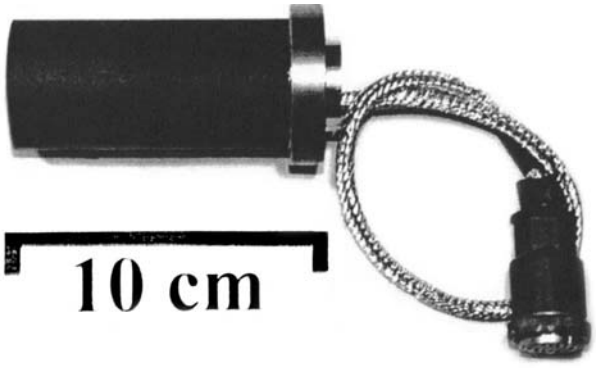

FIG. 5. View of the von Hamos spectrometer.

where σ is the standard deviation of the measurement. Assuming the dominant noise source is photon shot noise, σ is proportional to $(N_1)^{1/2}$. The sensitivity, N_1, determined in this way is indicated in Table I. The quantum efficiency is defined as

$$\text{QE} = \text{number of photons depleted/number of incidence photons} = N_1/N_0. \quad (4)$$

The values of QE obtained are presented in the last column in Table I. The QE values are in good agreement with the data[18,19] if we assume the CCD Si layer thickness equals ~ 20 μm. To estimate the CCD sensitivity at other photon energies it is useful to express the sensitivity N of each pixel in units of (e^-/count):

$$N = N_1 E/\epsilon, \quad (5)$$

because each depleted photon with energy E(eV) produces $E(\text{eV})/\epsilon$ electron–hole pairs ($\epsilon = 3.65$ eV is the energy for creation of one electron–hole pair in silicon at room temperature). From experimental data we have $N = 58.6e^-/\text{count}$ for $E = 1465$ eV (Mg target) and $N = 73.6e^-/\text{count}$ for $E = 4800$ eV (Ti target). The average value equals $N = 66e^-/\text{count}$ ($\pm 10\%$). The sensitivity N_0 (photons/count) for photon energy E is equal to

$$N_0(\text{photons/count}) = N_1/\text{QE} = N/\text{QE}\varepsilon/E = 66/\text{QE}\epsilon/E. \quad (6)$$

The quantum efficiency is estimated as a fraction of incidence flux absorbed in a 20-μm-thick Si layer:

$$\text{QE} = 1 - T = 1 - \exp(-\mu\rho l), \quad (7)$$

where T is the transmission of the Si layer, $\mu(E)$ is the mass absorption coefficient, $\rho = 2.32$ (g/cm^3) is the Si specific weight, and $l = 20$ μm is the Si layer thickness. Equation (5) can be used to estimate the detection limit $n_{\min}$ (photons/pixel). For dark current noise $3\sigma = 20$ counts,

$$n_{\min}(\text{photons/pixel}) = 20(\text{count})N_0(\text{photons/count}) = 1320/\text{QE}\epsilon/E. \quad (8)$$

The $n_{\min}$ (photons/pixel) values for some photon energies E(eV) are presented in Table II.

TABLE II. Detection limit $n_{\min}$ (photons/pixel) for a CCD linear array, efficiency B(ster) of the von Hamos spectrometer (mica crystals, n is reflection order), and minimum radiation yield $Y_{\min}$ (photons/sr) for several wavelengths (photon energies).

λ,Å	E,eV	$n_{\min}$ (photons/pixel)	$B(10^{-7}$ sr)[a]	$Y_{\min}$ (a/8 photons/sr)
8.7	1425	4.2	5.1(n=I)	8.2×10^6
2.6	4800	1.1	56(n=III)	2.0×10^5
1.85	6700	1.8	160(n=V)	1.1×10^5
1.5	8270	2.5	~100 (n=V)	2.5×10^5

[a]References 7 and 9.

C. von Hamos spectrometer

Curved mica ($2d = 19.84$ Å) and graphite ($2d = 6.708$ Å) crystals with radius of curvature $R = 20$ mm were used in the von Hamos spectrometer. The mica crystal was bent elastically on a cylindrical holder. The highly oriented pyrolytic graphite (HOPG) (Ref. 20) was bent plastically on a special cylindrical holder with the same radius of curvature. Some crystal parameters in the curved geometry—measured using a ^{55}Fe isotope source ($\lambda = 2.103$ Å),[10]—are presented in Table III. The mica-integrated reflectivity for different wavelengths ($\lambda = 1.84$–10 Å) and in different diffraction orders ($n = I$–V) was measured earlier using laser-produced plasmas.[7] The spectrometer (see Fig. 5) was installed in a standard 2 in. optical mount. The spectrometer axis was aligned along the target surface (Fig. 2). Spectra of highly charged ions were recorded using the calibrated CCD positioned in the image plane. To prevent visible light illumination, a double Al-coated mylar filter (4.4 μm of mylar, 0.2 μm of Al) was used. Spectra were recorded in a single laser shot. To avoid CCD saturation, Al filters of different thick-

TABLE III. Some crystal parameters in the curved geometry ($R = 20$ mm), measured by the ^{55}Fe isotope source ($\lambda = 2.103$ Å) (see Ref. 10).

Crystal	Thickness	Integrated reflectivity, ρ	Peak reflectivity	Rocking curve width
Mica, third-order reflection (effective $2d = 19.84/3 = 6.61$ Å)[a]	20 μm	4.06×10^{-2} mrad	No data	No data
Graphite ($2d = 6.708$ Å)[b]	100 μm	125×10^{-2} mrad	0.5	0.5°

[a]Manufacturer: Mica factory, Saint-Petersburg, Russia.
[b]Manufacturer: Optigraph Company, Moscow, Russia.

nesses (up to 73 μm) were used to attenuate the x-ray exposure on the CCD. The filtered intensity was up to 1/125 of the incidence intensity.

Spectra were recorded in the first, second, and fifth mica diffraction orders and in the first graphite diffraction order. The known crystal reflectivities, together with the CCD absolute calibration data, allowed us to record the spectra on an absolute intensity scale.

Using the calibration data and Eqs. (1) and (3), the radiation yield of the source in a monochromatic line can be estimated. For a source size $a<200$ μm, the CCD linear array covers the source image. In the dispersion direction, the source image occupies a (μm)/8 CCD pixels (8 μm is the pixel width). Integrating over the source size gives

$$Y = na/8\ 1/B, \tag{9}$$

where Y (photons/sr) is the radiation yield of the source in the monochromatic line, n (photons/pixel) is the CCD signal, and a (μm) is the source size. The minimum radiation yield $Y_{\min}$, which can be detected using the von Hamos spectrometer, is defined by the detection limit $n_{\min}$ of the CCD (see Table II):

$$Y_{\min} = n_{\min} a/8\ 1/B. \tag{10}$$

The values of parameter B and minimum yield $Y_{\min}$ for some wavelengths are presented in Table II. For arbitrary wavelength $Y_{\min}$ can be estimated using Eqs. (5) and (4) and data for parameter B.[7,10]

The spectral range $\Delta\lambda$ in our case is defined by the CCD length: $l=30$ mm. For this length and the spectrometer radius $R=20$ mm, the wavelength bandwidth $\Delta\lambda$ can be rather wide: $\Delta\lambda/\lambda=0.25-0.37$ for $\theta=20°-40°$. This spectral bandwidth is sufficient for x-ray plasma diagnostics (see the next section) and extended x-ray absorption fine structure (EXAFS) measurements ($\Delta\lambda/\lambda=0.1-0.2$).

IV. RESULTS

The x-ray spectra of highly charged ion excited in laser-produced plasmas are shown in Figs. 6 and 7. The spectra were recorded using the von Hamos spectrometer with mica (Figs. 6 and 7) and graphite (Fig. 7) crystals.

The peak reflectivity ratio (~4) for graphite and mica crystal is in good agreement with the data[10] obtained with the same crystals. The integrated reflectivity ratio for the same crystal is two times lower. The reason is that the CCD detects only part of the reflected x-ray radiation: the image of the source (~350–400 μm) caused by mosaic defocusing in the direction perpendicular to the dispersion is approximately twice as large as the CCD pixel height (200 μm).

Spectral resolution was calculated by the width of isolated lines. The spectral resolving power $\lambda/\delta\lambda$ in the von Hamos spectrometer is defined by the combined influence of the source size, the rocking curve width of the crystals and the line broadening in the plasma.[7] The contribution of these factors to the observed spectral resolution was not investigated in this work.

X-ray spectra obtained with the mica crystal show high spectral resolution: the spectral resolving power $\lambda/\delta\lambda$ was

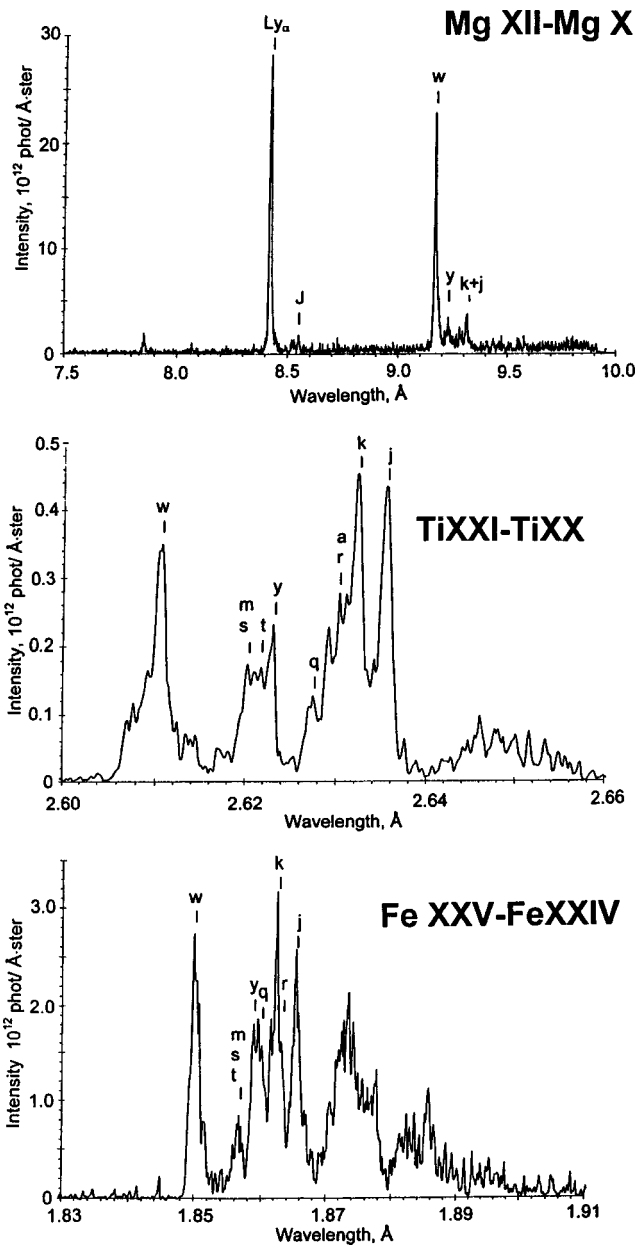

FIG. 6. Examples of x-ray spectra recorded by the von Hamos spectrometer with mica crystal: Mg spectrum (laser pulse energy $E_L=0.17$ J, first diffraction order $n=$I); Ti spectrum ($E_L=0.17$ J, $n=$III); and Fe spectrum ($E_L=2.3$ J, $n=$V).

equal to 800, 2000, and 2000 for Mg (first diffraction order), Ti (third diffraction order), and Fe (fifth diffraction order) plasmas, correspondingly (see Fig. 6). In the spectrum of the Ti plasma recorded by the graphite crystal (Fig. 7), the spectral resolving power is lower: $\lambda/\delta\lambda=200-300$. Nevertheless, due to mosaic parafocusing this value is higher than $\lambda/\delta\lambda=50$ defined by the mosaic spread of the graphite crystal.[10]

The high spectral resolution of the mica crystal von Hamos spectrometer allowed us to observe the complete satellite structure in spectra: *w*, *y*, resonance and intercombination lines of the He-like ions; *k*, *j*, dielectric satellites; and other (*m*, *s*, *t*; *q*; *a*, *r*) satellite lines (Gabriel's notation for satellite lines was used).[21] The line intensity ratios were used for plasma diagnostics. Using the intensity ratio, *w/y*, the elec-

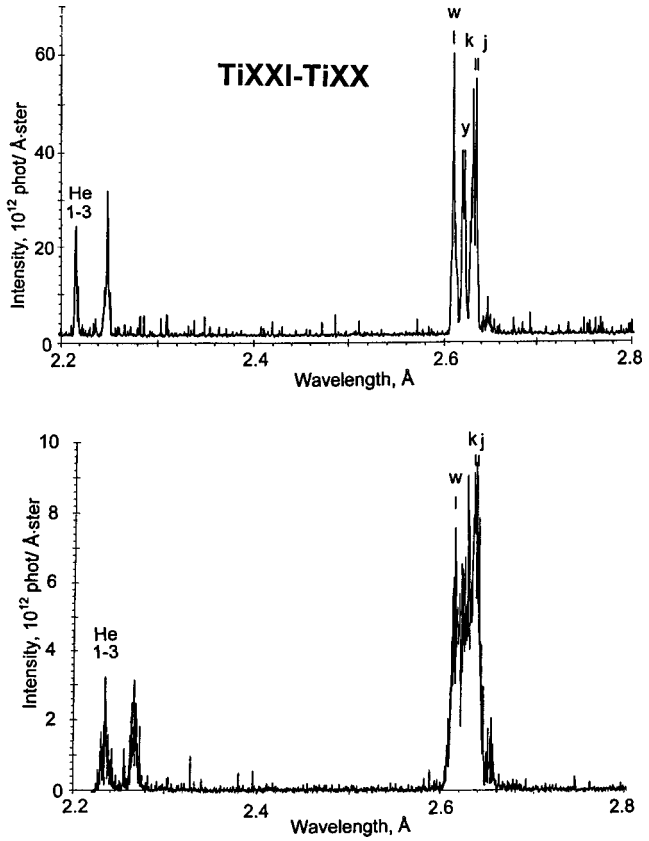

FIG. 7. Spectra of Ti laser-produced plasmas recorded by the von Hamos spectrometer with mica (at the top, laser pulse energy $E_L = 3.5$ J, third mica diffraction $n = \mathrm{III}$) and graphite (at the bottom, $E_L = 1$ J, $n = \mathrm{I}$) crystals.

tron density, N_e, was determined for the Mg laser-produced plasma:[22] $N_e = 3 \times 10^{20}$ cm^{-3}. Using the intensity ratio of dielectronic satellites j, k to the resonance line w the electron temperature T_e was measured.[23] The highest $T_e = 1400$ eV was observed in the Fe laser-produced plasma; the lowest $T_e = 150$ eV was measured in the Mg laser-produced plasma. Note that the spectra were observed at very low laser pulse energies (as low as 40 mJ for Mg plasmas). In most cases it was necessary to apply severe attenuation to the incidence x-ray intensity to avoid CCD saturation. Thus, the spectrometer is good for studying the x-ray spectra of low-intensity sources: femtosecond laser-produced plasmas, micropinches, EBIT sources, etc. The spectrometer could also be used for diagnostics of laser-produced plasma intended for extreme ultraviolet (EUV) lithography[24,25] at laser intensities on the target of $5 \times 10^{11} - 10^{12}$ W/cm^2.

The very high efficiency of the von Hamos spectrometer with the CCD linear array as a detector makes it possible to use the device in x-ray fluorescence (XRF) applications.[26] In this case the CCD must be cooled to reduce the dark current noise in order to measure low photon signals during long exposures. When the CCD is cooled from 20 ° to −30 °C, the dark current noise over an integrating time of 5 min corresponds to the exposure of 7 photons/pixel at a photon energy of 4.8 keV. Thus, a compact spectrometer for XRF applications should be possible.

In conclusion, this compact device is promising for absolute spectral measurement of x-ray radiation from low-intensity sources and for numerous practical applications (x-ray fluorescence analysis, EXAFS, etc.).

ACKNOWLEDGMENTS

The authors are grateful to E. G. Silkis (Institute of Spectroscopy) and A. A. Antonov and I. G. Grigorieva (Optigraph Company) for excellent technical help. The authors also gratefully acknowledge the invaluable assistance of Q. Wang (Brigham Young University) and A. A. Malyutin (Institute of General Physics). This work was supported by Brigham Young University, the P. N. Lebedev Physical Institute, and the Russian Fund for Fundamental Research (Grant No. 00-02-16632).

[1] *Charge-Transfer Devices in Spectroscopy*, edited by J. V. Sweedler, K. L. Ratzlaff, and M. B. Denton (Wiley, New York, 1994).
[2] A. J. D. Theuwissen, *Solid-State Imaging with Charge-Coupled Devices* (Kluwer Academic, Boston, MA, 1995).
[3] J. Dunn, B. K. F. Young, and J. Shiromizu, Rev. Sci. Instrum. **66**, 706 (1995).
[4] M. Koenig, J. M. Boudenne, P. Legriel, A. Benuzzi, T. Grandpierre, D. Batani, S. Bossi, S. Nicolella, and R. Benattar, Rev. Sci. Instrum. **68**, 2387 (1997).
[5] F. Blasco, C. Stenz, F. Salin, A. Ya. Faenov, A. I. Magunov, T. A. Pikuz, and I. Yu. Skobelev, Rev. Sci. Instrum. **72**, 1956 (2001).
[6] L. von Hámos, Ann. Phys. **17**, 716 (1933).
[7] A. P. Shevelko, Proc. SPIE **3406**, 91 (1998).
[8] B. Yaakoby, R. E. Turner, H. W. Schnopper, and P. O. Taylor, Rev. Sci. Instrum. **50**, 1609 (1979).
[9] B. Yaakoby and A. J. Burek, IEEE J. Quantum Electron. **19**, 1841 (1983).
[10] A. P. Shevelko, A. A. Antonov, I. G. Grigorieva, Yu. S. Kasyanov, L. V. Knight, A. Reyes-Mena, C. Turner, Q. Wang, and O. F. Yakushev, Proc. SPIE **4144**, 148 (2000).
[11] F. Bijkerk, E. Louis, G. E. van Dorssen, A. P. Shevelko, and A. A. Vasilyev, Appl. Opt. **32**, 4247 (1993).
[12] C. R. Vane, M. Smith, S. Raman, J. Heard, and T. Walkiewics, Nucl. Instrum. Methods Phys. Res. B **24/25**, 56 (1987).
[13] J. Hoszowska, J.-Cl. Dousse, J. Kern, and Ch. Rhême, Nucl. Instrum. Methods Phys. Res. A **376**, 129 (1996).
[14] E. Källne and J. Källne, Phys. Scr., T **3**, 185 (1983).
[15] P. Beiersdorfer, R. E. Marrs, J. R. Henderson, D. A. Knapp, M. A. Levine, D. B. Platt, M. B. Schneider, D. A. Vogel, and K. L. Wong, Rev. Sci. Instrum. **61**, 2338 (1990).
[16] G. E. Ice and C. J. Sparks, Nucl. Instrum. Methods Phys. Res. A **291**, 110 (1990).
[17] B. L. Henke, F. G. Fujiwara, M. A. Tester, C. H. Dittmore, and M. A. Palmer, J. Opt. Soc. Am. B **1**, 828 (1984).
[18] A. Saemann and K. Eidmann, Rev. Sci. Instrum. **69**, 1949 (1998).
[19] L. Poletto, A. Boscolo, and G. Tondello, Appl. Opt. **38**, 29 (1999).
[20] A. A. Antonov, V. B. Baryshev, I. G. Grigoryeva, G. N. Kulipanov, and N. N. Shchipkov, Nucl. Instrum. Methods Phys. Res. A **308**, 442 (1991).
[21] A. H. Gabriel, Mon. Not. R. Astron. Soc. **160**, 99 (1972).
[22] A. V. Vinogradov, I. Yu. Skobelev, and E. A. Yukov, Sov. J. Quantum Electron. **5**, 630 (1975).
[23] L. A. Vainshtein, U. I. Safronova, and A. M. Urnov, in *Proceedings of the Lebedev Physical Institute,* edited by N. G. Basov (Nova Science, New York, 1980), Vol. 119.
[24] G. Kubiak, L. J. Bernardez, K. Krenz, W. C. Replogle, W. C. Sweatt, D. W. Sweeney, R. M. Hudyma, and H. Shields, Proc. SPIE **3767**, 136 (1999).
[25] R. C. Constantinescu, J. Jonkers, P. Hegeman, and M. Visser, Proc. SPIE **4146**, 101 (2000).
[26] D. C. Turner, L. V. Knight, A. Reyes-Mena, P. W. Moody, H. K. Pew, J. D. Phillips, A. P. Shevelko, S. Voronov, and O. F. Yakushev, Adv. X-Ray Anal. **44**, 257 (2000).